# A rod-like mesoporous carbon derived from agro-industrial cassava petiole waste for supercapacitor application

*by* Rika Taslim

**Submission date:** 07-Dec-2020 10:40AM (UTC+0700)
**Submission ID:** 1466953954
**File name:** 2020-Taer_E-Journal_of_Chemical_Technology_and_Nanotechnolgy.pdf (4.57M)
**Word count:** 8250
**Character count:** 42930

Research Article

Received: 14 May 2020 Revised: 7 September 2020 Accepted article published: 26 September 2020 Published online in Wiley Online Library:

(wileyonlinelibrary.com) DOI 10.1002/jctb.6579

# A rod-like mesoporous carbon derived from agro-industrial cassava petiole waste for supercapacitor application

**Erman Taer,[a*] Apriwandi Apriwandi,[a] Bima Kumala Levanadea Dalimunthe[a] and Rika Taslim[b]**

## Abstract

**BACKGROUND: Agro-industrial co-products rich in lignocellulose, for example cassava petiole (CP) waste, have high potential as sources of porous carbon materials, alongside other impressive advantages, including ease of acquisition, abundance and availability, renewability and low cost. This work shows the successful treatment of mesoporous carbon with rod-like structure derived from agro-industrial CP waste carbonized and physically activated by direct one-stage integrated pyrolysis using a zinc chloride ($ZnCl_2$) activator agent, in the production of a supercapacitor electrode for energy storage. $ZnCl_2$ was tested at varying concentrations, including 0.5, 0.7 and 0.9 mol $L^{-1}$. The surface morphology, chemical content, surface area and porous size distribution were evaluated to determine the physical properties of activated carbon, and a cyclic voltammetry method was used to assess the electrochemical characteristics using a two-electrode system in 1 mol $L^{-1}$ $H_2SO_4$ as an electrolyte.**

**RESULTS: The porous carbon obtained displayed a rod-like morphology structure, featuring numerous hierarchical tuneable well-confirmed micropores and mesopores. This monolithic material contained predominantly C (87.85%), demonstrating a maximum surface area of 759.816 $m^2$ $g^{-1}$ at 0.9 mol $L^{-1}$ concentration. Furthermore, the highest specific capacitance reached was 193 F $g^{-1}$ at 0.7 mol $L^{-1}$, with maximum energy and power densities of 26.90 Wh $kg^{-1}$ and 96.94 W $kg^{-1}$, respectively.**

**CONCLUSION: The novel rod-like mesoporous carbon derived from CP waste produced using a facile, cost-effective and sustainable method, without metal–organic framework or templates, shows great potential as an electrode material for enhanced supercapacitor performance.**


**Keywords:** porous carbon; cassava petiole waste; electrode material; supercapacitor

## INTRODUCTION

The current evolution in industry and technology is having an impact on most sectors, and on daily routines globally. The energy consumption worldwide was estimated to be increasing consistently by 2.9% in 2019,[1] underlining the urgent need for sustainable use of fossil fuels, alongside concerns about the impacts on global climate change and pollution hazards.[2,3] These concerns are encouraging research towards the development of renewable energy systems, as well as possible storage and conversion systems. There is a need to improve the efficiency of storage systems, particularly in line with the increase in demand, as the costs to shift to alternative sources are relatively high. Supercapacitors recently have demonstrated exceptional performance as an entity with the capacity to store green energy, based on the extremely fast charge–discharge, high power density, unlimited long-term stability, low cost and easier relative production processes.[4] Supercapacitors are divided into two types, on the basis of storage mechanisms, including (i) electrochemical double layer capacitors (EDLC), which accumulate charges through the adsorption of fast electrolyte ions on the surface of the electrodes, by forming an electrochemical double layer, and (ii) pseudocapacitance, where storage is attained by faradaic redox reactions, at the electrode–electrolyte interface.[4,5] However, supercapacitors are known to possess relatively low energy density, and possible improvement through various means has been a topic for intense research.[6,7]

Several previously adopted techniques include the development and modification of new materials with excellent capacitive performance. Porous carbon is one of the materials believed to possess promisingly strong performance because of the increased specific surface area, suitable pore size distribution, nanostructures and hierarchical porosity of surface morphology,[8,9] good chemical stability and processing ease.[10] Furthermore, an increase in energy density requires porous carbon with a hierarchical porosity, obtainable from micro-, meso-, as well as macropores.[11] The macroporous structure specifically provides low-realistic distance for ion diffusion on the electrode

* Correspondence to: E Taer, Department of Physics, University of Riau, 28293 Simpang Baru, Riau, Indonesia. E-mail: erman_taer@yahoo.com

a Department of Physics, University of Riau, Simpang Baru, Indonesia

b Department of Industrial Engineering, State Islamic University of Sultan Syarif Kasim, Simpang Baru, Indonesia

 

surface, subsequently enhancing the supercapacitor rate.[12] In addition, mesopores create relatively smooth ion transport pathways devoid of obstacles to the electrode–electrolyte interface, whereas micropores provide a large surface area to increase the amount of active sites for ion diffusion, which allows for an increased formation of double-layer ions.[13,14] The pores interconnected from all three tend to achieve a capacitor performance with high energy density. However, many researchers have reported that hierarchical porous carbon still requires relatively more expensive production costs and raw materials that are difficult to obtain.

Agriculture and agro-industrial wastes rich in lignocellulose have high potential as sources of porous carbon materials, alongside other impressive advantages, including their ease of acquisition, abundance and availability, renewability and low cost.[15,16] Meanwhile numerous reports have shown the potential for adopting agricultural and agro-industrial wastes in the development of hierarchical pores and modification of the surface morphology supercapacitor electrodes.[17–19] This was recently demonstrated in a study by Yang *et al.*, which reported on the modification of carbon obtained from mangosteen waste, using carbonization methods, followed by activation with sodium hydroxide (NaOH).[20] The resulting material possessed a surface area of 2623 $m^2 g^{-1}$, with excellent specific capacitance of 357 F $g^{-1}$. Similar results were shown by carbon from maya waste and basil seed produced using potassium hydroxide (KOH) activation, which gave a surface area of 11[illegible]–1870 $m^2 g^{-1}$, and specific capacitance of 255–464 F $g^{-1}$.[21,22] Porous carbon was synthesized from cotton waste, through swelling, using NaOH/urea solution and a pyrolysis process, resulting in highly hierarchical porous nanofibers with a specific capacitance of 221 F $g^{-1}$.[23] Furthermore, modification of surface morphology with ellipsoidal structure and rod-like shape of biomass-based carbon were reported by Sun *et al.* and Jiang *et al.* using aluminum-based metal organic frameworks; their studies resulted in large surface areas of 1400–1886 $m^2 g^{-1}$ which enhanced the specific capacitance to 306.4–345 F $g^{-1}$.[24,25] These preparations, however, require the addition of adhesives and other synthetic materials (e.g. PTFE) with metal frameworks, which inhibit the attainment of maximum capacitive properties.

In this study, porous activated carbon with a rod-like shape was synthesized from the agro-industrial co-product cassava petiole (CP) waste, with $ZnCl_2$ activation, followed by direct one-stage integrated pyrolysis involving both carbonization and physical activation methods. This activated carbon was prepared entirely from basic waste, in a monolithic form, without adding adhesives and other synthetic materials or any metal organic frameworks or any templates. Low concentrations of $ZnCl_2$ (0.5, 0.7 and 0.9 mol $L^{-1}$) were selected to maintain the self-adhesive nature of the raw material. Based on analysis by scanning electron microscopy (SEM) and $N_2$ gas adsorption/desorption analyses, the monolithic carbon exhibited rod-like structure and hierarchical, tuneable, well-confirmed mesopores, resulting from the greater surface area and graded porous structure. This product displayed excellent electrochemical performance, with specific capacitance, energy and high power densities of 193 F $g^{-1}$, 26.90 Wh $kg^{-1}$ and 96.94 W $kg^{-1}$, respectively.

## MATERIALS AND METHODS

### The preparation of porous activated carbon

Agro-industrial cassava petiole (CP) wastes were obtained from the traditional market in Riau province, which was then washed, cut and sundried for two days. Subsequently, pre-carbonization was conducted in an oven at a temperature of 250 °C for 2.5 h, followed by grinding and milling to produce homogenous powder. This sample was then sieved to produce particle sizes of 53 μm, and consequently activated by chemical activation with the three different $ZnCl_2$ concentrations (0.5, 0.7 and 0.9 mol $L^{-1}$, labeled CP-0.5, CP-0.7 and CP-0.9, respectively). The activated carbon powder was changed into monolithic form using a hydraulic press. All samples were subjected to one-stage integrated pyrolysis, with carbonization at 600 °C temperature in an $N_2$ gas environment, and physical activation using $CO_2$ gas atmosphere, at 900 °C for 2.5 h (see one-stage integrated pyrolysis profile in Fig. 1). The final step involved the rearrangement of a supercapacitor cell into sandwich type, consisting of carbon electrodes, electrolyte, current collector and separator. Figure 1 shows the porous activated carbon synthesis for the supercapacitor cell.

### Characterization of physical properties

The physical properties, including density, degree of crystallinity, morphology, chemical composition, surface area and pore size distribution were determined. Furthermore, sample density was calculated based on the mass, diameter and volume of the monolithic carbon, whereas the thermal stability of pre-carbonized powder samples were reviewed using Thermo-gravimetric (TG; DTG, derivatives TG) analysis (TGA-50 instrument, Shimadzu, Kyoto, Japan) at a heating rate of 10 °C $min^{-1}$ in an $N_2$ gas atmosphere with flow rate 100 mL $min^{-1}$. Moreover, X-ray diffraction (XRD, X'Pert Pro PW3060/10 instrument, Malvern panalytical, Malvern, UK) was used to evaluate the degree of crystallinity, interlayer spacing ($d_{002}$ and $d_{100}$) based on Bragg's Law and microcrystallite dimensions ($L_c$ and $L_a$, respectively) were calculated using the Debey–Scherer equation [Eqns (1) and (2)].[26] Scanning electron microscopy (JSM-6510LA, JEOL, Tokyo, Japan) was applied to review the surface morphology at a voltage of 15 kV, whereas chemical compositions were analyzed with energy dispersive spectroscopy (EDS, JSM-6510LA, JEOL) at the energy range 0–20 KeV. In addition, the pores characteristics including the Brunauer–Emmett–Teller (BET) specific surface areas and pore size distributions (PSD) were observed using a $N_2$ gas asorption method (TouchWin v1.2 instrument, Quantachrome Corp., Boynton Beach, FL, USA), at liquid nitrogen temperature of 77 K. PSD were calculated using the Barret–Joiner–Halenda (BJH) method.

$$L_c = \frac{0.89\lambda}{\beta cos\theta_{002}} \quad (1)$$

$$L_a = \frac{1.94\lambda}{\beta cos\theta_{100}} \quad (2)$$

### Electrochemical measurements

The supercapacitor cell was assembled in the sandwich form, consisting of the two electrodes free and binderless, with separator from a egg duck shell membrane and 1 mol $L^{-1}$ $H_2SO_4$ electrolyte. The electrodes were prepared by polishing the carbon monolith CPs which had been pyrolyzed to 0.2 mm thickness and placed in two pieces without binder materials. The specific capacitances of the CPs were obtained through computation using cyclic voltammetry (CV, UR Rad-Er 5841 instrument, Pekanbaru, Indonesia, calibrated by VersaStat II Princeton Applied Research, an error of ±6.05%) curve areas, at a potential window of 0.0 to 1.0 V with 1 mV $s^{-1}$, 5 mV $s^{-1}$ and 10 mV $s^{-1}$ scan rates in the 1 mol $L^{-1}$



  

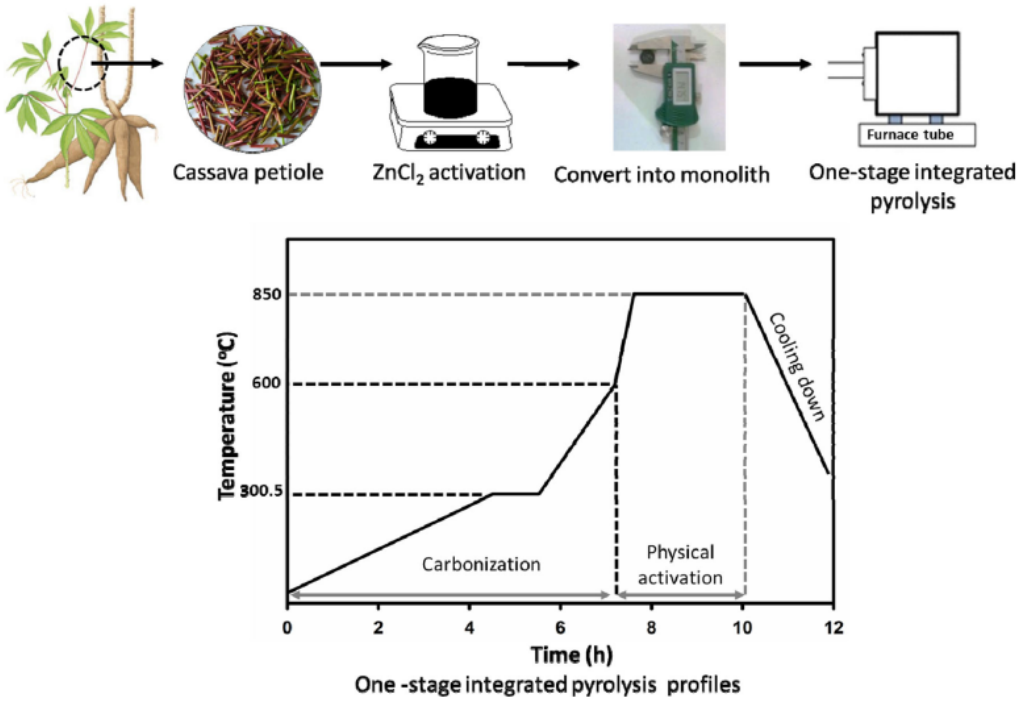


**Figure 1.** Preparation scheme of porous activated carbon.

$_4$ aqueous electrolyte. The values of specific capacitance ($C_{sp}$, F g$^{-1}$), energy density ($E$, Wh kg$^{-1}$) and power density ($P$, W kg$^{-1}$) were obtained using the following standard equations:[27,28]:

$$Csp = \frac{I}{s \times m} \quad (3)$$

$$I = \frac{2(Ic - Id)}{2} \quad (4)$$

$$E = \frac{1}{2} pV^2 \frac{1}{3.6} \quad (5)$$

$$P = \frac{E}{\Delta t} \times 3600 \quad (6)$$

$I_c$ is the current density when charged and $I_d$ is the current density when discharged (both A cm$^{-2}$), $s$ is scan rate (mV s$^{-1}$), $m$ is average mass of electrodes (g), $V$ is voltage (V) and $\Delta t$ is the discharged time (s).

## RESULTS AND DISCUSSION

### Thermogravimetric and density analyses

The pyrolysis profiles for both carbonization and physical activation are important factors in the conversion of the CP porous activated carbon. The purpose of carbonization was to reduce the volatile content and produce high fixed carbon content, whereas the physical activation led to suitable pore development. The pyrolysis profile could be assessed intuitively from the TG/DTG curves in Fig. 2. Thermogravimetric analysis was performed to investigate the degree of thermal degradation directly related to thermal stability by a simple approach. This correlates the weight lost at different temperature intervals, following a heat treatment, to the total loss obtained after conventional thermal treatment, and the data obtained are subsequently used for predictions. Figure 2 shows the TG and the DTG profiles in the $N_2$ gas atmosphere for pre-carbonized CP powder. This demonstrates three stages of maximum weight loss, corresponding to the moisture content, volatility and complexity of the compound. The first stage was evaluated at a temperature of 105 °C, which features drying, evaporation and the de-volatilization of water, minerals and moisture.[29] Therefore, the second stage showed a maximum weight loss of 38.81% at ≈200 °C, attributed to the degradation of hemicellulose and cellulose, which continued up to 38[illegible]C. The third stage demonstrated a loss of ≈56.70%, which was observed at a temperature range of 430–600 °C, related to the release of $CO_2$ and $CH_4$.[30] These are emitted due to the decomposition of

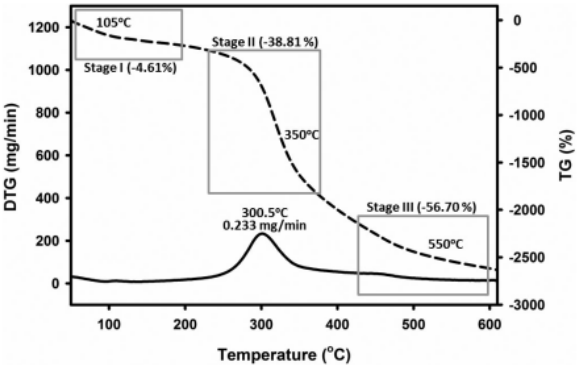


**Figure 2.** TG and DTG profiles of pre-carbonized CP powder.

cellulose as well as lignin, which specifically continued at higher temperatures (900 °C). Therefore, the optimal carbonization temperature at which the cassava petiole could be pyrolyzed more effectively was 600 °C. The pyrolysis profile is shown in detail in Fig. 2(b). The DTG profile showed significant decomposition rate of the pre-carbonized sample in the temperature range 30–600 °C, the highest rate of weight loss was at 300.5 °C, corresponding to decomposition of hemicellulose, cellulose and lignin. Subsequently, CO, $CO_2$, $H_2O$ and $CH_4$[30,31] were released simultaneously, causing sharp peaks on the DTG profile, at a weight loss rate of 0.233 mg $min^{-1}$. This is in line with the TG profile which showed significant weight loss in the 200–380 °C range, and also correlates with other carbon biomass-based studies.[32,33] Therefore, 300.5 °C was considered thermally stable for the decomposition of moisture, volatile and complex compounds of CP, and selected for use as the initial resistance temperature for the carbonization process [see Fig. 2(b)].

Density was analyzed first to predict pore properties and morphology, as well as the capacitive behaviors of monolithic carbon, based on biomass materials, in the production of supercapacitor electrodes.[33,34] This parameter was evaluated by measuring the mass, diameter and thickness of the samples, which became relatively smaller after pyrolysis. This reduction was caused by the dehydration of impurities, subsequently increasing material porosity, leading to a decline in density. This phenomenon caused the retention of more ions on the pores, therefore influencing the production of higher energy density, which was 0.692 g $cm^{-3}$ for CP-0.7 followed by 0.597 g $cm^{-3}$ and 0.563 g $cm^{-3}$ for CP-0.9 and CP-0.5, respectively (Fig. 3), after pyrolysis. The most significant specific capacitance was identified for CP-0.7, which does not correspond with the theoretical assumptions, likely as a consequence of pore blockade, preventing the ions from occupying the pores. Therefore, the fact that CP-0.5 had the highest density was not an indicator of highest specific capacitance. In addition, $ZnCl_2$ was selected as an activator because of its intrinsic function of being a dehydration agent, facilitating the release of hydrogen and oxygen present in the raw material into the air in the form of vaporized water at high temperatures. This led to an increase in the disorder of samples,[35] as the carbonization process was initiated at temperatures between 30 °C and 600 °C, a range associated with the decomposition of hemicelluloses (200–380 °C), cellulose (250–380 °C) and lignin (380–900 °C) based on TG/DTG analysis. Conversely, physical activation was introduced because of the bigger pores caused by hydroxylation, and subsequent reduction in sample mass. This phenomenon ensued because of the decline in density, and also corroborates other previously reported studies.[33,34]

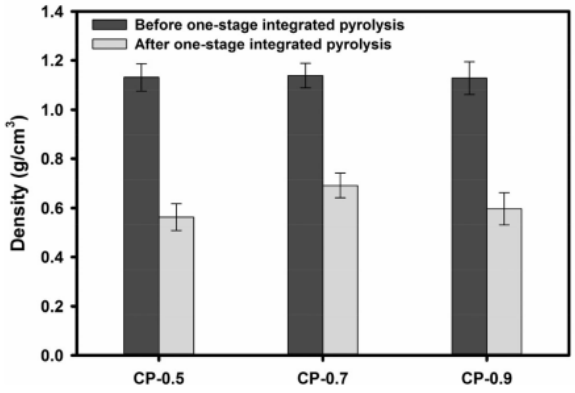


**Figure 3.** The density of carbon electrodes before and after one-stage pyrolysis.

### Morphology structure and degree of crystallinity

Figure 4 shows the surface morphology of monolithic carbon derived from CP, impregnated using three different $ZnCl_2$ concentrations, identified by SEM. This impregnation procedure, alongside the one-stage pyrolysis, led to the decomposition of hemicellulose, cellulose and lignin releasing CO, $CO_2$ and $CH_4$[30] from the raw material, subsequently developing the pores and structure morphology of monolithic samples. In addition, the one-stage integrated pyrolysis both of carbonization and physical activation, successfully etched and decomposed the three complex compounds at different temperatures, including hemicellulose (200–380 °C), cellulose (250–380 °C) and lignin (380–900 °C).[30] Moreover, ZnOCl as a co-product of $ZnCl_2$ activation decomposed first, leading to the possible formation of macropores, whereas the $CO_2$ and $H_2O$ produced as final products etched the production of mesopores and micropores.

Generally, the SEM images for all samples show aggregations and rod-like shapes with meso- and macropores on the surface of the monolithic carbon. Figure 4(a) demonstrates the aggregations in the morphologies with relatively larger sizes, at 0.96–3.55 µm, possessing correlative macropores with widths of 215 nm. Figure 4(b) shows the presence of rod-like shapes with length and diameter of 3.32 µm and 0.63 µm, respectively, whereas Fig. 4(c) demonstrates similarity in morphologies with aggregation reduction into smaller sizes of 0.23–1.58 µm and macropores also declined to the size of mesopores with widths of ≈485 nm. Based on the SEM magnification, several rod-like shapes were identified for CP-0.7 [Fig. 4(d)], with lengths and diameters of 1.73–3.14 µm and 0.55–0.74 µm, respectively. This increased the potential of obtaining an hierarchical combination of macropores and mesopores, subsequently promoting the free access of ions to the material surface, shuttling across the channels.[36]

The further increase in $ZnCl_2$ concentration for CP-0.9 [Fig. 4(e)] led to the formation of morphologies with smaller aggregations, correlating with macropores and mesopores measuring 1.55 µm and 0.27 µm in length and diameter, respectively [Fig. 4(f)]. This structure was characterized by high porosity and increased specific surface area, alongside the rod-like shapes, existing as fine structure, owing to the aggregation of decomposed cellulose, hemicellulose and lignin from the direct pyrolysis process.[25] These components, except cellulose were originally globular in shape,[25,37,38] which were modified after treatment at 600 °C, although lignin exhibited minimal changes after 800 °C. Meanwhile, the reduction in rod-like shapes and macropore structures was due to activation by $ZnCl_2$, which firstly formed the co-product 'ZnOCl', enabling the generation of more final products, including $CO_2$ and $H_2O$ on decomposition. This resulted in reduced pore width and the production of numerous rod-like shapes small in size. Therefore, cellulose and hemicellulose are assumed to be very potent in the generation of 3D and interconnected porous structures, giving rise to increased surface area and suitable pores, and subsequently contributing to high rates of ion diffusion into electrode supercapacitors. This unique morphology structure is similar to that described in other reports which used different methods and approaches.[24,25,39,40]



  

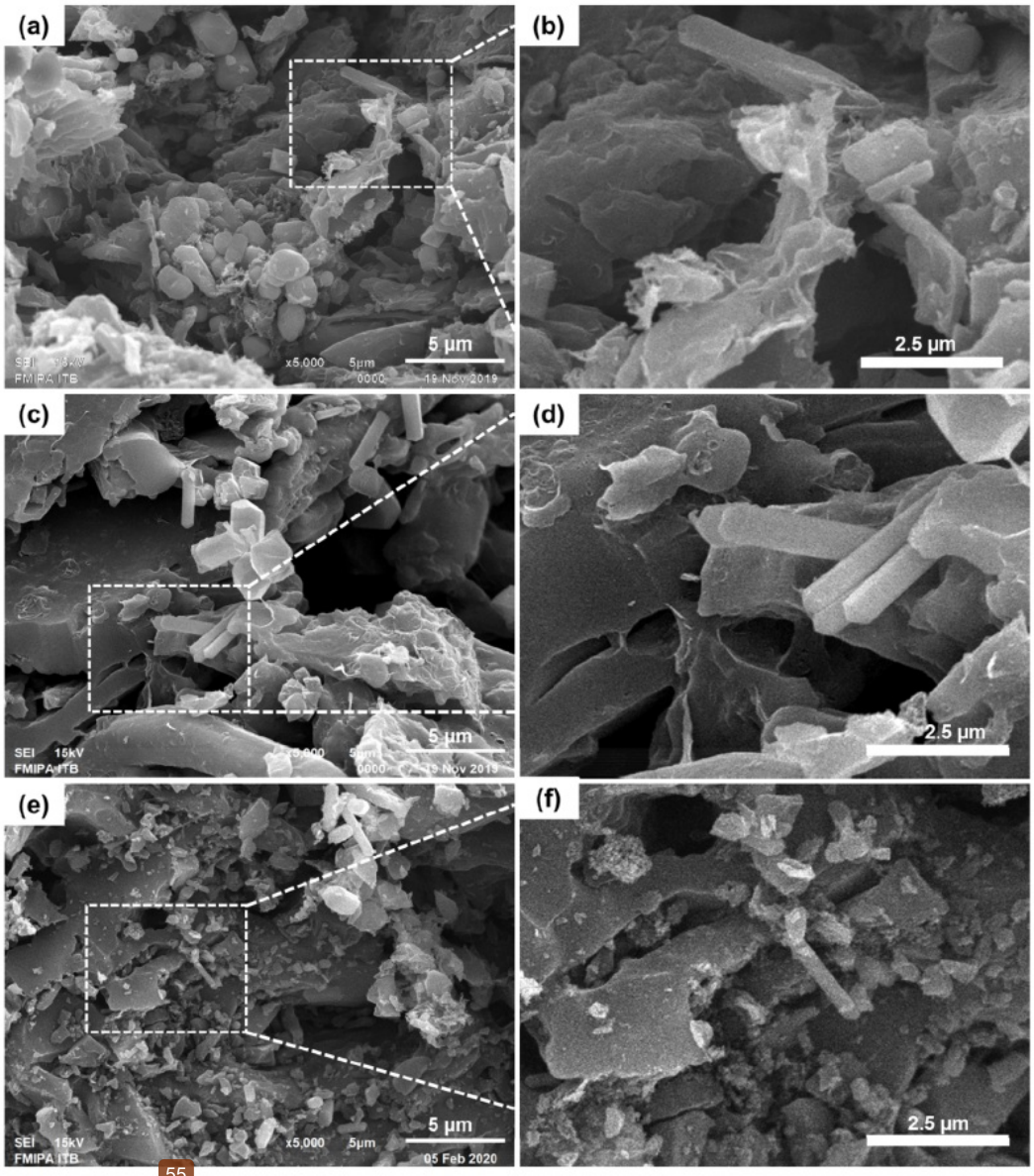


**Figure 4.** SEM images for (a) CP-0.5, (b) enlarged detail of CP-0.5, (c) CP-0.7, (d) enlarged detail of CP-0.7, (e) CP-0.9 and (f) enlarged detail of CP-0.9.

The degree of crystallinity in the carbon monolith structure was elucidated by XRD measurement, as illustrated in Fig. 5. This shows the XRD patterns based on three different concentrations of $ZnCl_2$ introduced as chemical activation agents. All samples contained two broad peaks at $2\theta$ = 24–25° and $2\theta$ = 44–45°, which are related to the (002) and (100) planes of carbon (JCPDS nos 41–1487).[24,41,42] This characteristic is attributed to the presence of a relatively highly amorphous structure, which is very common in carbonaceous materials. The (002) plane corresponds to hexagonal configuration, whereas the (100) diffraction is the in-plane graphitic structure of activated carbon. Other biomass-based carbon materials demonstrating similar behavior include durian shell,[43] banana stem[44] and mangosteen,[20] although the XRD peak broadness was observed to have largely reduced from CP-0.5 to CP-0.9. This is indicative of a structure transition from amorphous to graphitic, following the addition of $ZnCl_2$.[39] The XRD pattern also showed several sharp peaks at 32–33°, 36.6°, 38° and 49°, which signify the presence of $Ca_5(PO_4)_3Cl$ (chloropatite), MgO (magnesium oxide) and $CaCO_3$ (Calcium carbonate). It was found that the activator concentrations only minimally influenced the reduction of impurities present in the monolithic carbon, which existed in higher amounts based on the XRD patterns of CP-0.5 to CP-0.9. These impurities in the samples were extracted from the basic elements of CP biomass as confirmed by EDS analysis (see Table 2), and are believed to exhibit pseudocapacitance behavior, which subsequently increases supercapacitor

  

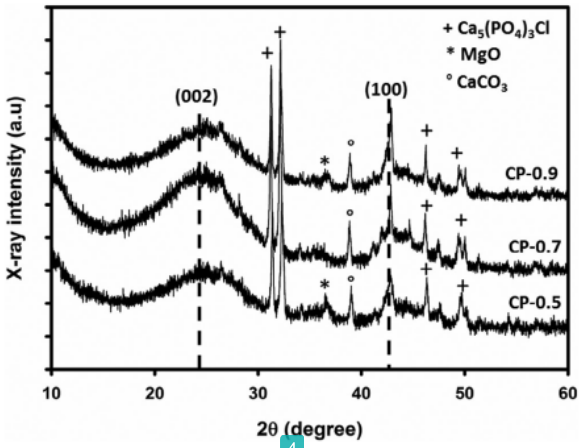


**Figure 5.** The XRD patterns of the CP-0.5, CP-0.7 and CP-0.9 samples.

performance. This assumption was confirmed by the CV profile discussed in the Chemical composition subsection below.

Table 1 shows a detailed report on (i) interlayer spacing, including ($d_{002}$ and $d_{100}$), considered normal for amorphous carbon structures from biomass raw materials,[45] and (ii) lattice parameters ($L_a$ and $L_c$) obtained from the Debye–Sheerer formula [Eqns (1) and (2)]. These data are within the typical range for carbon materials, as the $L_c$ shows an indirect correlation with the surface area, which is calculated using the formula $S = 2\rho/L_c$.[46,47] This evaluation is confirmed by the $N_2$ gas absorption analysis, which also demonstrates an increase in surface area.

## Chemical composition

The chemical composition of activated carbon samples were studied using energy dispersive spectroscopy. Table 2 shows the chemical composition of monolithic carbon, based on the three different concentrations of $ZnCl_2$. These samples were generally dominated by carbon, alongside several other components. Moreover, the one-stage pyrolysis process, characterized by carbonization and physical activation was completely successful in the conversion of CP biomass into activated carbon, comprising high percentages of the carbon element (87–92.66%). This elevated proportion implies the removal of most volatile and noncarbon content from the sample during pyrolysis.[48] Furthermore, the addition of $ZnCl_2$ as an activator agent at 0.5–0.7 mol $L^{-1}$ led to an increased carbon percentage, possibly because of the effective decomposition of noncarbon compounds, including organic acids, volatiles and tar. However, the CP-0.9 samples treated with $ZnCl_2$ demonstrated a reduction in carbon elements by 86.66%. Conversely, the oxygen content gradually increased from 7.00–9.23 to 0.5–0.9 mol $L^{-1}$, indicating an increase in hydrophilic behavior, featuring improved wettability and an enhanced pseudocapacitance effect of samples.[49] In addition, the low levels of Ca, K and Mg contribute to the basic component of organic materials,[50] whereas the Cl content responsible for the submaximal neutralization of samples, originated from the $ZnCl_2$ activator. This analysis corroborated findings from the XRD analysis, which stated the existence of $Ca_5(PO_4)_3Cl$, MgO and $CaCO_3$ in all samples.

**Table 2.** The percentage chemical composition of activated carbon made from CP

| Element | Atomic weight (%) CP-0.5 | CP-0.7 | CP-0. |
|---|---|---|---|
| Carbon | 87.07 | 87.85 | 86.66 |
| Oxygen | 7.00 | 8.03 | 9.23 |
| Magnesium | 0.50 | 0.88 | 0.78 |
| Chlorine | 0.72 | 0.98 | 0.93 |
| Calcium | 1.62 | 2.26 | 2.40 |
| Iron | 3.09 | - | - |
| Totals | 100% | | |

## $N_2$ absorption

The $N_2$ gas adsorption/desorption method is commonly used to evaluate surface area and the pore size distribution of activated carbon derived from biomass materials. Furthermore, all samples tested showed a mixture of types I and IV isotherms, according to the IUPAC classification.[51,52] Hence, a significant increase in isotherms at a low relative ($P/P_0 < 0.1$) pressure is an indicator of micropore structures,[53] whereas the hysteresis loop at higher values ($0.4 < P/P_0 < 0.95$) designates the presence of numerous mesopores.[54] Subsequently, all of the samples exhibited well-developed combinations of micropores and mesopores, as seen in Fig. 6, where CP-0.5 consisted of loop type-IV isotherm, and CP-0.5 and CP-0.9 showed distortion. This indicates a limitation in the occurrence of ideal mesoporous structures to CP-0.5, which provided the proper porosity for fast ion diffusion and large surface area required to improve capacitive behavior. This loop hysteresis distortion occurred owing to the presence of ink-bottled shaped and numerous narrow neck pores. This thin nature hinders $N_2$ gas desorption because of pore constriction,[55] although $ZnCl_2$ chemical impregnation (0.5 to 0.9 mol $L^{-1}$) successfully enlarged the specific surface area to 495.08 $m^2\ g^{-1}$ (CP-0.5), 632.19 $m^2\ g^{-1}$ (CP-0.7) and 759.81 $m^2\ g^{-1}$ (CP-0.9). This manifestation clearly proves that $ZnCl_2$ is a potential material for improving surface area and increasing the amount of pores, which is necessary in the creation of more active sites for ion diffusion at the electrode–electrolyte interface.

Figure 7 shows the PSD reviewed using BJH. This parameter indicates the dominant pore diameter of the carbon monolith, within the range 3.5–20 nm. Hence, all samples are believed to

**Table 1.** The interlayer spacing ($d_{002}$ and $d_{100}$) and lattice parameters $L_c$ and $L_a$ for carbon electrodes of CP

| Monolithic carbon | $2\theta_{002}$ (°) | $2\theta_{100}$ (°) | $d_{002}$ (Å) | $d_{100}$ (Å) | $L_a$ (Å) | $L_c$ (Å) |
|---|---|---|---|---|---|---|
| CP-0.5 | 25.369 | 44.828 | 3.508 | 2.020 | 7.021 | 11.140 |
| CP-0.7 | 24.664 | 45.173 | 3.606 | 2.005 | 17.951 | 10.790 |
| CP-0.9 | 23.456 | 45.742 | 3.766 | 1.998 | 19.543 | 9.560 |



  

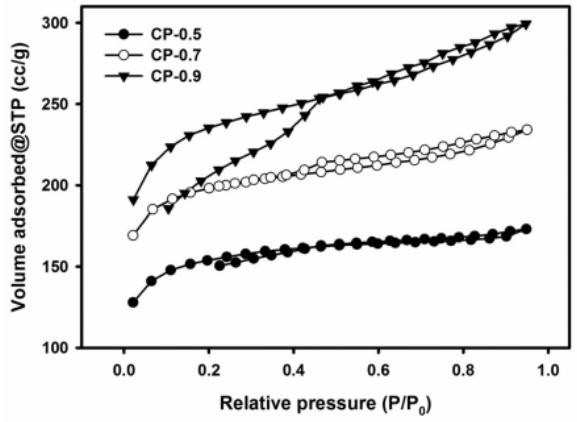


**Figure 6.** The $N_2$ gas isotherm for monolithic carbon derived from CP.

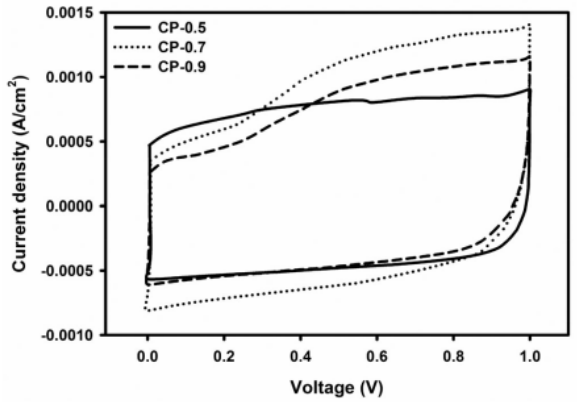


**Figure 8.** The CV curve for each monolithic carbon electrode derived from CP waste.

consist mesopores with interconnected structures,[36,51,56] which led to low-resistance pathways for ions diffusion at the inner pore surface.[36] However, sample CP-0.9 demonstrated better mesopore dominance than CP-0.5 and CP-0.7, which indicates superior specific surface area. This structure is assumed to be capable of providing stable capacitive behavior for supercapacitor electrodes, being a characteristic associated with improved ion diffusion. This analysis was proven in the electrochemical behavior discussed in the next subsection. Also, all results, including specific surface area and pore size distribution for this study were similar to those for substrates analyzed in other research, such as pitaya waste[21] and rice husk.[57]

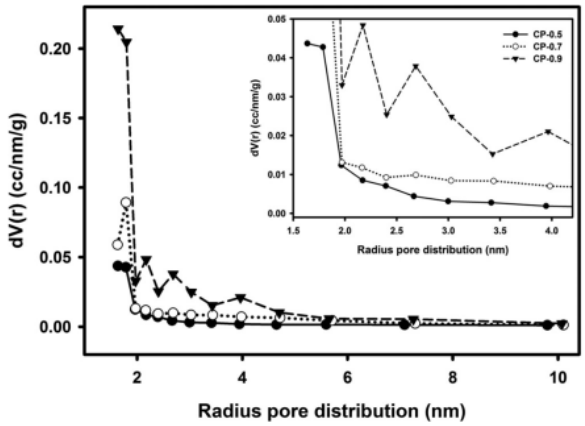


**Figure 7.** The pore size distribution for monolithic carbon samples derived from CP.

Table 3 shows a summary of the pore properties of the CP samples. Notably, when the concentration of $ZnCl_2$ increased from 0.5 to 0.9 mol $L^{-1}$, the specific surface area ($S_{BET}$) and total pore volume ($V_{tot}$) increased from 495.08 $m^2$ $g^{-1}$ to 759.81 $m^2$ $g^{-1}$ and 0.27 $cm^3$ $g^{-1}$ to 0.46 $cm^3$ $g^{-1}$, respectively. Furthermore, the mesopore surface ($S_{meso}$) and mesopore volume ($V_{meso}$) also increased, and micropore formation reduced. This condition is expected to increase the degree of wall collapse between adjacent pores during physical activation, leading to an enlargement of the larger ones, evidenced by the increase in average pore diameter ($D_{aver}$). For further analysis, the micropore surface ($S_{micro}$) was well defined as a deviation of specific surface area, whereas the development of mesopores contributed to a reduction in the ion storage pathway, leading to high power density. Therefore, hierarchical and tuneable well-confirmed micropores and mesopores are expected to produce the best electrochemical performance, as predicted for CP-0.7.

### Cyclic voltammetry analysis

Cyclic voltammetry is a popular method used to evaluate the electrochemical behavior of the carbon electrode supercapacitor, including specific capacitance, energy and power density. The resulting curve demonstrates a correlation between the potential windows and the $I_c$ (charge)–$I_d$ (discharge) current density data. Figure 8 illustrates the CV curves for all samples evaluated with 1 mV $s^{-1}$ scan rates, at 0–1.0 V window voltage, with a two-electrode system. Therefore, 1 mol $L^{-1}$ $H_2SO_4$ was selected as an electrolyte, and all samples treated with different activator concentrations showed the ideal quasi-rectangular shape observed in electrochemical double-layer capacitors derived from biomass materials.[58] The CV CP-0.7 and CP-0.9 curves present a clear redox peak with distorted rectangular shape at 0.2–0.4 V, indicating the behavior of the electrochemical double layer alongside the

**Table 3.** The pore characteristics of three CPs

| Samples | $S_{BET}$ ($m^2$ $g^{-1}$) | $S_{micro}$ ($m^2$ $g^{-1}$) | $S_{meso}$ ($m^2$ $g^{-1}$) | $V_{tot}$ ($cm^3$ $g^{-1}$) | $V_{micro}$ ($cm^3$ $g^{-1}$) | $V_{meso}$ ($cm^3$ $g^{-1}$) | $D_{aver}$ (nm) |
|---|---|---|---|---|---|---|---|
| CP-0.5 | 495.08 | 468.64 | 26.44 | 0.27 | 0.32 | 0.03 | 2.28 |
| CP-0.7 | 632.19 | 582.83 | 49.36 | 0.36 | 0.16 | 0.06 | 2.29 |
| CP-0.9 | 759.81 | 625.20 | 134.61 | 0.46 | 0.13 | 0.16 | 2.44 |

**Table 4.** Specific capacitance, energy and power density measurements at 1 mV $s^{-1}$ scan rate for each monolithic carbon electrodes samples

| Sample codes | $C_{sp}$ (F $g^{-1}$) | $E$ (Wh $kg^{-1}$) | $P$ (W $kg^{-1}$) |
|---|---|---|---|
| CP-0.5 | 152.49 | 21.18 | 76.32 |
| CP-0.7 | 193.68 | 26.90 | 96.94 |
| CP-0.9 | 186.15 | 25.85 | 93.15 |

impact of pseudocapacitance. These pseudoproperties are indicated from the sample composition of $Ca_5(PO_4)_3Cl$, MgO and $CaCO_3$, as confirmed in the XRD and EDS analysis, which was not identified in the CP-0.5 samples. Furthermore, the specific capacitance, energy and power density were determined using formulae (3), (4), (5) and (6) shown in Table 4.

The specific capacitance values of CP-0.5, CP-0.7 and CP-0.9 were 152.49 F $g^{-1}$, 193.68 F $g^{-1}$ and 186.15 F $g^{-1}$, respectively, where 0.5–0.7 mol $L^{-1}$ is assumed to be affected by the $ZnCl_2$ concentration. Also, the capacitance initially demonstrated an increase, followed by a subsequent decline, alongside the addition of $ZnCl_2$, with 0.7 mol $L^{-1}$ exhibiting the highest values. However, higher concentrations were ascertained to increase the speed of activation, leading to the formation of more pores, tunable micropores/mesopores and increased surface areas. This, therefore, increased the amount of diffusion ions on the activated carbon electrodes in the electrolytic solution, resulting in elevated specific capacitance. Hence CP-0.7 was concluded to exhibit the highest value, despite it not having higher specific surface area owing to a well-developed combination of micropores/mesopores and the functional rod-like structure, which promotes ion diffusion into the inside pores.[25] In addition, concentrations greater than 0.7 augmented the activation rate, leading to over-etching and consequent expansion of the final pore sizes. This led to a reduction in micropore volume, as well as the specific capacitance of the activated carbon electrode.

Figure 9(a) shows the CV curves of CP-0.7 at different scan rates, ranging from 1 mV $s^{-1}$ to 5 mV $s^{-1}$, revealing that the rectangular shapes were observed to possess greater stability with a gradual increase in scan rate. These characteristics indicate excellent capacitor behavior of the carbon electrode materials examined. Figure 9(b) also demonstrates the directly proportional relationship between specific capacitance and scan rate, varied at 1, 2, 5 and 10 mV $s^{-1}$, which was observed for all the samples. Conversely, a decline in specific capacitance was attributed to a

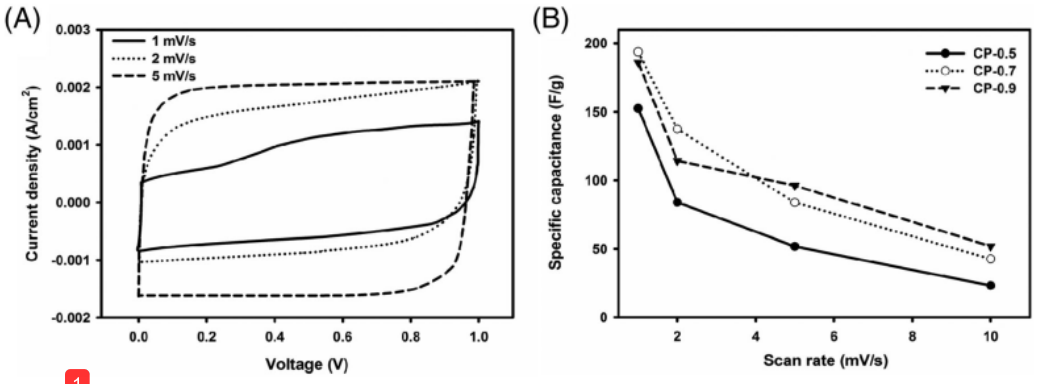


**Figure 9.** (a) The specific capacitance *versus* scan rate variations for all samples, and (b) scan rate variations for CP-0.7 samples.

**Table 5.** The comparison of various biomass based-activated carbon as supercapacitor electrodes

| Material sources | Morphology structures | Activator agents | $S_{BET}$ ($m^2$ $g^{-1}$) | Electrolyte | $C_{sp}$ (F $g^{-1}$) | $E$ (Wh $kg^{-1}$) | $P$ (W $kg^{-1}$) | Ref |
|---|---|---|---|---|---|---|---|---|
| Bamboo | 3D-porous | KOH | 2221.1 | 3 mol $L^{-1}$ KOH | 293 | 10.9 | 63 | 54 |
| Sakura Flower | Honeycomb-like shape | KOH | 1785.41 | 6 mol $L^{-1}$ KOH | 265 | - | - | 60 |
| Banana Peel | Hierarchical porous | $ZnO_3$ | 1650 | 6 mol $L^{-1}$ KOH | 206 | - | - | 61 |
| $(Al(OH)_3)$ | Ellipsoidal structure | - | 1400 | 6 mol $L^{-1}$ KOH | 306.4 | - | - | 24 |
| $(AlCl_3.6H_2O)$ | Rod-like shape | KOH-$KNO_3$ | 1886 | 6 mol $L^{-1}$ KOH | 345 | - | - | 25 |
| Apiaria | Nanofibers | KOH | 1280 | 6 mol $L^{-1}$ KOH | 324 | 11 | 60 | 62 |
| Fructose Corn Syrup | Spherical structure | - | 1473 | 6 mol $L^{-1}$ KOH | 168 | 42 | 1500 | 63 |
| Wool Felt | Tubular structure | - | 438 | 2 mol $L^{-1}$ $H_2SO_4$ | 152 | - | - | 64 |
| Tobacco | 3D-porous | KOH | 1297.6 | 6 mol $L^{-1}$ KOH | 148 | 2.66 | 51 | 35 |
| Rotten Carrot | Heterogeneous structure | $ZnCl_2$ | 1119.56 | 1 mol $L^{-1}$ $LiClO_4$ | 142.7 | 28.4 | 89.1 | 52 |
| Cassava Petiole | Rod-like shape | $ZnCl_2$ | 759.81 | 1 mol $L^{-1}$ $H_2SO_4$ | 193 | 26.90 | 96.94 | This study |



  

variety of controlling factors, including pore-size distribution, the combination of micro- and mesopores, as well as specific surface area.[11,59] Specifically, CP-0.9 exhibited the best rate dependence with 70% of 74 F $g^{-1}$, attained at the scan rate of 10 mV $s^{-1}$, whereas CP-0.5 and CP-0.7 showed a similar trend with ~76% of 61 and 32 F $g^{-1}$, respectively, and at the scan rate of 10 mV $s^{-1}$. This was influenced by the pores which dominated the carbon electrode samples. The CP-0.7 sample was dominated by micropores which hampered the electrolyte ion flow at higher scanning rates leading to the worse rate capability of the samples. Table 5 shows the high similarity between the specific capacitance results of other materials and CP.

## CONCLUSION

In conclusion, hierarchical porous carbon obtained from CP was successfully prepared through a multi-step method, using $ZnCl_2$ as an activator agent which was followed by one-stage directly integrated pyrolysis, featuring carbonization and physical activation. The resulting material exhibited rod-like shapes with hierarchically porous morphology, comprising suitable micro-, meso- and macropores, and all samples became highly amorphous in structure. Furthermore, other crystal compounds identified, including $Ca_5(PO_4)_3Cl$, MgO and $CaCO_3$ correlated with the capacitive behavior of the samples. The addition of varying $ZnCl_2$ concentrations led to changes in the specific surface area, as seen in CP-0.9 which demonstrated a gradual increase in value from 495 $m^2$ $g^{-1}$ to 759.816 $m^2$ $g^{-1}$, with characteristic average pore diameter of 3.27 nm. Furthermore, the symmetric cell supercapacitor exhibited a high specific capacitance of 193 F $g^{-1}$ in two-electrode system energy density. This pseudocapacitance behavior was observed in CP-0.7 and CP-0.9, although the supercapacitors were stabilized at the higher concentration of $ZnCl_2$ (0.9 mol $L^{-1}$), with a rate dependence of 70%. These results indicate the high potential of adopting agro-industrial CP waste-based porous carbon materials as supercapacitor energy storage.

## ACKNOWLEDGEMENTS

The authors would like to thank the DRPM Kemenristek-Dikti through the second year project of PD (396/UN.19.5.1.3/PT.01.03/2020) with the title 'High-density micro-and nano carbon fiber made from biomass based materials for supercapacitor electrodes'.

## REFERENCES

1 BPSTATS, Review of World Energy Statistical Review of World, 68th edition, BP Statistical Review of World Energy, pp 1–69 (2019). Available: https://www.bp.com/content/dam/bp/business-sites/en/global/corporate/pdfs/energy-economics/statistical-review/bp-stats-review-2019-full-report.pdf
2 Höök M and Tang X, Depletion of fossil fuels and anthropogenic climate change-A review. *Energy Policy* **52**:797–809 (2013).
3 WHO, *COP24 Special Report Health and Climatec Change*. World Health Organization, Geneva, pp. 1–74 (2018).
4 Burke A, Ultracapacitors: why, how, and where is the technology. *J Power Sources* **91**:37–50 (2000).
5 Iro ZS, Subramani C and Dash SS, A brief review on electrode materials for supercapacitor. *Int J Electrochem Sci* **11**:10628–10643 (2016).
6 González A, Goikolea E, Barrena JA and Mysyk R, Review on supercapacitors: Technologies and materials. *Renew Sustain Energy Rev* **58**:1189–1206 (2016).
7 Thomas P, Lai CW and Bin Johan MR, Recent developments in biomass-derived carbon as a potential sustainable material for supercapacitor-based energy storage and environmental applications. *J Anal Appl Pyrolysis* **140**:54–85 (2019).
8 Pandolfo AG and Hollenkamp AF, Carbon properties and their role in supercapacitors. *J Power Sources* **157**:11–27 (2006).
9 Jose J, Thomas V, Vinod V, Abraham R and Abraham S, Nanocellulose based functional materials for supercapacitor applications. *J Sci Adv Mater Devices* **4**:333–340 (2016).
10 Kim J, Won H, Min S, Jae J and Park Y, Overview of the recent advances in lignocellulose liquefaction for producing biofuels, bio-based materials and chemicals. *Bioresour Technol* **279**:373–384 (2019).
11 Yang S, Wang S, Liu X and Li L, Biomass derived interconnected hierarchical micro-meso-macro- porous carbon with ultrahigh capacitance for supercapacitors. *Carbon* **147**:540–549 (2019).
12 Zhang Y, Yu S, Lou G, Shen Y, Chen H, Shen Z *et al.*, Review of macroporous materials as electrochemical supercapacitor electrodes. *J Mater Sci* **52**:11201–11228 (2017).
13 Song T, Liao JM, Xiao J and Shen LH, Effect of micropore and mesopore structure on $CO_2$ adsorption by activated carbons from biomass. *Xinxing Tan Cailiao/New Carbon Mater* **30**:156–166 (2015).
14 Wu J, Xia M, Zhang X, Chen Y, Sun F, Wang X *et al.*, Hierarchical porous carbon derived from wood tar using crab as the template: performance on supercapacitor. *J Power Sources* **455**:227982 (2020).
15 Yahya MA, Al-qodah Z and Ngah CWZ, Agricultural bio-waste materials as potential sustainable precursors used for activated carbon production: A review. *Renew Sustain Energy Rev* **46**:218–235 (2015).
16 Zhu J, Yan C, Zhang X, Yang C, Jiang M and Zhang X, A sustainable platform of lignin: from bioresources to materials and their applications in rechargeable batteries and supercapacitors. *Prog Energy Combust Sci* **76**:100788 (2020).
17 Yang W, Shi Z, Guo H, Guo J, Lei X and Yue L, Study on preparation of nanocarbon fibers from wheat-straw based on electrostatic spinning method and its application in supercapacitor. *Int J Electrochem Sci* **12**:5587–5597 (2017).
18 Cai Y, Luo Y, Dong H, Zhao X, Xiao Y, Liang Y *et al.*, Hierarchically porous carbon nanosheets derived from *Moringa oleifera* stems as electrode material for high-performance electric double-layer capacitors. *J Power Sources* **353**:260–269 (2017).
19 Azwar E, Wan Mahari WA, Chuah JH, Vo DVN, Ma NL, Lam WH *et al.*, Transformation of biomass into carbon nanofiber for supercapacitor application-A review. *Int J Hydrogen Energy* **43**:20811–20821 (2018).
20 Yang V, Senthil RA, Pan J, Khan A, Osman S, Wang L *et al.*, Highly ordered hierarchical porous carbon derived from biomass waste mangosteen peel as superior cathode material for high performance supercapacitor. *J Electroanal Chem* **855**:113616 (2019).
21 Lu W, Cao X, Hao L, Zhou Y and Wang Y, Activated carbon derived from pitaya peel for supercapacitor applications with high capacitance performance. *Mater Lett* **264**:127339 (2020).
22 Yang H, Zhou J, Wang M, Wu S, Yang W and Wang H, From basil seed to flexible supercapacitors: green synthesis of heteroatom-enriched porous carbon by self-gelation strategy. *Int J Energy Res* **44**:4449–4463 (2020).
23 Liu Y, Shi Z, Gao Y, An W, Cao Z and Liu J, Biomass-swelling assisted synthesis of hierarchical porous carbon fibers for supercapacitor electrodes. *ACS Appl Mater Interfaces* **8**:28283–28290 (2018).
24 Sun Y, Guo S, Li W, Pan J, Fernandez C, Arumugam R *et al.*, A green and template-free synthesis process of superior carbon material with ellipsoidal structure as enhanced material for supercapacitors. *J Power Sources* **405**:80–88 (2018).
25 Jiang W, Pan J and Liu X, A novel rod-like porous carbon with ordered hierarchical pore structure prepared from Al-based metal-organic framework without template as greatly enhanced performance for supercapacitor. *J Power Sources* **409**:13–23 (2019).
26 Valente Nabais JM, Teixeira JG and Almeida I, Development of easy made low cost bindless monolithic electrodes from biomass with controlled properties to be used as electrochemical capacitors. *Bioresour Technol* **102**:2781–2787 (2011).
27 Sun Q, Jiang T, Zhao G and Shi J, Porous carbon material based on biomass prepared by MgO template method and $ZnCl_2$ activation method as electrode for high performance supercapacitor. *Int J Electrochem Sci* **14**:1–14 (2019).
28 Men B, Guo P, Sun Y, Tang Y, Chen Y, Pan J *et al.*, High-performance nitrogen-doped hierarchical porous carbon derived from cauliflower for advanced supercapacitors. *J Mater Sci* **54**:2446–2457 (2019).
29 Fan Y, Cai Y, Li X, Jiao L, Xia J and Deng X, Effects of the cellulose, xylan and lignin constituents on biomass pyrolysis characteristics and bio-

  

oil composition using the Simplex Lattice Mixture Design method. *Energ Conver Manage* **138**:106–118 (2017).
30 Gonzalez J, Roma S, Encinar JM and Martı G, Pyrolysis of various biomass residues and char utilization for the production of activated carbons. *J Anal Appl Pyrolysis* **85**:134–141 (2009).
31 De Luna MY, Rodrigues PM, Antônia G, Torres M, Antônio J, Queiroz MJ *et al.*, A thermogravimetric analysis of biomass wastes from the northeast region of Brazil as fuels for energy recovery. *Energy Sources, Part A Recover Util Environ Eff* **41**:1557–1575 (2018).
32 Sellin N, Ricardo D, Marangoni C and Souza O, Oxidative fast pyrolysis of banana leaves in fluidized bed reactor. *Renew Energy* **96**:56–64 (2016).
33 Taer E, Apriwandi A, Taslim R, Malik U and Usman Z, Single step carbonization-activation of durian shells for producing activated carbon monolith electrodes. *Int J Electrocem Sci* **14**:1318–1330 (2019).
34 Taer E, Apriwandi A, Ningsih YS and Taslim R, Agustino, Preparation of activated carbon electrode from pineapple crown waste for supercapacitor application. *Int J Electrochem Sci* **14**:2462–2475 (2019).
35 Chen H, Guo YC, Wang F, Wang G, Qi PR, Guo XH *et al.*, An activated carbon derived from tobacco waste for use as a supercapacitor electrode material. *New Carbon Mater* **32**:592–599 (2017).
36 Wang Y, Qu Q, Gao S, Tang G, Liu K, He S *et al.*, Biomass derived carbon as binder-free electrode materials for supercapacitors. *Carbon* **155**:706–726 (2019).
37 Deng J, Xiong T, Wang H, Zheng A and Wang Y, Effects of cellulose, hemicellulose, and lignin on the structure and morphology of porous carbons. *ACS Sustain Chem Eng* **4**:3750–3756 (2016).
38 Rangabhashiyam S and Balasubramanian P, The potential of lignocellulosic biomass precursors for biochar production: Performance, mechanism and wastewater application-A review. *Ind Crops Prod* **128**:405–423 (2019).
39 Li Y, Wang X and Cao M, Three-dimensional porous carbon frameworks derived from mangosteen peel waste as promising materials for $CO_2$ capture and supercapacitors. *J CO2 Util* **27**:204–216 (2018).
40 Lam SS, Lee XY, Nam WL, Phang XY, Liew RK, Yek PNY *et al.*, Microwave vacuum pyrolysis conversion of waste mushroom substrate into biochar for use as growth medium in mushroom cultivation. *J Chem Technol Biotechnol* **94**:1406–1415 (2019).
41 Su X, Li S, Jiang S, Peng Z, Guan X and Zheng X, Superior capacitive behavior of porous activated carbon tubes derived from biomass waste-cotonier strobili fibers. *Adv Powder Technol* **29**:2097–2107 (2018).
42 Ramesh T, Rajalakshmi N, Dhathathreyan KS and Reddy LRG, Hierarchical porous carbon microfibers derived from Tamarind seed coat for high-energy supercapacitor application. *ACS Omega* **3**:12832–12840 (2018).
43 Ong LK, Kurniawan A, Suwandi AC, Lin CX, Zhao XS and Ismadji S, A facile and green preparation of durian shell-derived carbon electrodes for electrochemical double-layer capacitors. *Prog Nat Sci Mater Int* **22**:624–630 (2012).
44 Taer E, Taslim R, Mustika WS, Kurniasih B, Agustino A, Afrianda A *et al.*, Production of an activated carbon from a banana stem and its application as electrode materials for supercapacitors. *Int J Electrochem Sci* **13**:8428–8439 (2018).
45 Farma R, Deraman M, Awitdrus A, Talib IA, Taer E, Basri NH *et al.*, Preparation of highly porous binderless activated carbon electrodes from fibres of oil palm empty fruit bunches for application in supercapacitors. *Bioresour Technol* **132**:254–261 (2013).
46 Kumar K, Saxena RK, Kothari R, Suri DK, Kaushik NK and Bohra JN, Correlation between adsorption and x-ray diffraction studies on viscose rayon based activated carbon cloth. *Carbon* **35**:1842–1844 (1997).
47 Deraman M, Daik R, Soltaninejad S, Nor NSM, Awitdrus FR *et al.*, A new empirical equation for estimating specific surface area of supercapacitor carbon electrode from X-ray diffraction. *Adv Mater Res* **1108**:1–7 (2015).
48 Nasssar MM and Mackay GDM, Mechanism of thermal decomposition of lignin. *Wood Fiber Sci* **3**:441–453 (1984).
49 Wei H, Wang H, Li A, Li H, Cui D, Dong M *et al.*, Advanced porous hierarchical activated carbon derived from agricultural wastes toward high performance supercapacitors. *J Alloys Compd* **820**:153111 (2020).
50 Contescu CI, Adhikari SP, Gallego NC and Evans ND, Activated carbons derived from high-temperature pyrolysis of lignocellulosic Biomass. *J Carbon Res* **4**:9–13 (2018).
51 Sing KSW, Reporting physisorption data for gas/solid systems with special reference to the determination of surface area and porosity. *Pure Appl Chem* **54**:2201–2218 (1982).
52 Ahmed S, Ahmed A and Rafat M, Supercapacitor performance of activated carbon derived from rotten carrot in aqueous, organic and ionic liquid based electrolytes. *J Saudi Chem Soc* **22**:993–1002 (2018).
53 Muniandy L, Adam F, Rahman A and Ng E, The synthesis and characterization of high purity mixed microporous/mesoporous activated carbon from rice husk using chemical activation with NaOH and KOH. *Microporous Mesoporous Mater* **197**:316–323 (2014).
54 Zhang G, Chen Y, Chen Y and Guo H, Activated biomass carbon made from bamboo as electrode material for supercapacitors. *Mater Res Bull* **102**:391–398 (2018).
55 Ayinla RT, Dennis JO, Zaid HM, Sanusi YK, Usman F and Adebayo LL, A review of technical advances of recent palm bio-waste conversion to activated carbon for energy storage. *J Clean Prod* **229**:1427–1442 (2019).
56 Sodtipinta J, Ieosakulrat C, Poonyayant N, Kidkhunthod P, Chanlek N, Amornsakchai T *et al.*, Interconnected open-channel carbon nanosheets derived from pineapple leaf fiber as a sustainable active material for supercapacitors. *Ind Crops Prod* **104**:13–20 (2017).
57 He X, Ling P, Qiu J, Yu M, Zhang X, Yu C *et al.*, Efficient preparation of biomass-based mesoporous carbons for supercapacitors with both high energy density and high power density. *J Power Sources* **240**:109–113 (2013).
58 Scott K, Electrochemical principles and characterization of bioelectrochemical systems, in *Microbial Electrochemical and Fuel Cells*, ed. by Scott K and Yu EH. Woodhead, Cambridge, UK, pp. 29–66 (2016).
59 Zhang WL, Xu JH, Hou DX, Yin J, Liu DB, He YP *et al.*, Hierarchical porous carbon prepared from biomass through a facile method for supercapacitor applications. *J Colloid Interface Sci* **530**:338–344 (2018).
60 Ma F, Ding S, Ren H and Liu Y, Sakura-based activated carbon preparation and its performance in supercapacitor applications. *RSC Adv* **9**:2474–2483 (2019).
61 Lv Y, Gan L, Liu M, Xiong W, Xu Z, Zhu D *et al.*, A self-template synthesis of hierarchical porous carbon foams based on banana peel for supercapacitor electrodes. *J Power Sources* **209**:152–157 (2012).
62 Deng L, Zhong W, Wang J, Zhang P, Fang H, Yao L *et al.*, The enhancement of electrochemical capacitance of biomass-carbon by pyrolysis of extracted nanofibers. *Electrochim Acta* **228**:398–406 (2017).
63 Cao W and Yang F, Supercapacitors from high fructose corn syrup-derived activated carbons. *Mater Today Energy* **9**:406–415 (2018).
64 Pina A, Amaya A, Marcuzzo J, Rodrigues A, Baldan M, Tancredi N *et al.*, Supercapacitor electrode based on activated carbon wool felt. *J Carbon Res* **4**:24–36 (2018).



  

# A rod-like mesoporous carbon derived from agro-industrial cassava petiole waste for supercapacitor application

ORIGINALITY REPORT

| 19% | 9% | 18% | 6% |
|---|---|---|---|
| SIMILARITY INDEX | INTERNET SOURCES | PUBLICATIONS | STUDENT PAPERS |

PRIMARY SOURCES

| | | |
|---|---|---|
| 1 | Erman Taer, Verdy Manoto Naipospos, Rika Taslim, Agustino, Apriwandi. "Activated Carbon Monolith Derived from Coconut Husk Fiber as Electrode Material for Supercapacitor Energy Storage", Journal of Physics: Conference Series, 2020<br>Publication | 2% |
| 2 | Submitted to University Politehnica of Bucharest<br>Student Paper | 1% |
| 3 | Erman Taer, Martauli Sihombing, Rika Taslim, Agustino, Apriwandi. "Bamboo-Based Activated Carbon as Binder-Free Electrode of Supercapacitor Application", Journal of Physics: Conference Series, 2020<br>Publication | 1% |
| 4 | www.repositorio.ufrn.br:8080<br>Internet Source | 1% |
| 5 | Viengkham Yang, Raja Arumugam Senthil, Junqing Pan, Abrar Khan, Sedahmed Osman, | 1% |

Liren Wang, Wenchao Jiang, Yanzhi Sun. "Highly ordered hierarchical porous carbon derived from biomass waste mangosteen peel as superior cathode material for high performance supercapacitor", Journal of Electroanalytical Chemistry, 2019
Publication

---

6 Erman Taer, Friska Febriyanti, Widya Sinta Mustika, Rika Taslim, Agustino Agustino, Apriwandi Apriwandi. "Enhancing the performance of supercapacitor electrode from chemical activation of carbon nanofibers derived Areca catechu husk via one-stage integrated pyrolysis", Carbon Letters, 2020 — 1%
Publication

---

7 ruidera.uclm.es — <1%
Internet Source

---

8 Erman Taer, Agrandi Purnama, Apriwandi, Agustino, Rika Taslim, Widya Sinta Mustika. "An Optimization Method to Determine Optimum Carbonization Temperature of Banana Stems Based Activated Carbon for Supercapacitors", IOP Conference Series: Materials Science and Engineering, 2019 — <1%
Publication

---

9 Sara Bovina, Dario Frascari, Alessandro Ragini, Francesco Avolio, GianNicola Scarcella, Davide — <1%

Pinelli. "Development of a continuous-flow anaerobic co-digestion process of olive mill wastewater and municipal sewage sludge", Journal of Chemical Technology & Biotechnology, 2020
Publication

---

10 Zan Gao, Yunya Zhang, Ningning Song, Xiaodong Li. "Biomass-derived renewable carbon materials for electrochemical energy storage", Materials Research Letters, 2016 <1%
Publication

---

11 Apriwandi, Agustino, Erman Taer, Rika Taslim. "A High Potential of Biomass Leaves Waste for Porous Activated Carbon Nanofiber/Nanosheet as Electrode Material of Supercapacitor", Journal of Physics: Conference Series, 2020 <1%
Publication

---

12 Zhibin Yang, Jing Ren, Zhitao Zhang, Xuli Chen, Guozhen Guan, Longbin Qiu, Ye Zhang, Huisheng Peng. "Recent Advancement of Nanostructured Carbon for Energy Applications", Chemical Reviews, 2015 <1%
Publication

---

13 Zhi-Qiang Hao, Jing-Pei Cao, Yan Wu, Xiao-Yan Zhao, Li Zhou, Xing Fan, Yun-Peng Zhao, Xian-Yong Wei. "Preparation of porous carbons from waste sugar residue for high performance <1%

electric double-layer capacitor", Fuel Processing Technology, 2017
Publication

| | | |
|---|---|---|
| 14 | royalsocietypublishing.org<br>Internet Source | <1% |
| 15 | E Taer, P Kurniawan, R Taslim, A Agustino, Apriwandi, A Afrianda. "Carbon electrode based on durian shell: effects concentration of chemical activator agent (Potassium hydroxide)", Journal of Physics: Conference Series, 2018<br>Publication | <1% |
| 16 | Machado Yguatyara de Luna, Ponte Marcelo Rodrigues, Gadelha Antônia Mabrysa Torres, da Costa Júnior Antônio Eufrázio et al. "A thermogravimetric analysis of biomass wastes from the northeast region of Brazil as fuels for energy recovery", Energy Sources, Part A: Recovery, Utilization, and Environmental Effects, 2018<br>Publication | <1% |
| 17 | Agrawal, Richa, Chunhui Chen, Yong Hao, Yin Song, and Chunlei Wang. "Graphene for Supercapacitors", Graphene-based Energy Devices, 2015.<br>Publication | <1% |
| 18 | Yuan Gao, Qinyan Yue, Baoyu Gao, Aimin Li. | |

| | | |
|---|---|---|
| | "Insight into activated carbon from different kinds of chemical activating agents: A review", Science of The Total Environment, 2020<br>Publication | <1% |
| 19 | Shirley Palisoc, Joshua Marco Dungo, Michelle Natividad. "Low-cost supercapacitor based on multi-walled carbon nanotubes and activated carbon derived from Moringa Oleifera fruit shells", Heliyon, 2020<br>Publication | <1% |
| 20 | Chenrayan Senthil, Chang Woo Lee. "Biomass-derived biochar materials as sustainable energy sources for electrochemical energy storage devices", Renewable and Sustainable Energy Reviews, 2020<br>Publication | <1% |
| 21 | dalspace.library.dal.ca<br>Internet Source | <1% |
| 22 | Duo Liu, Shuai Yu, Yalun Shen, Hao Chen, Zhehong Shen, Shuyan Zhao, Shenyuan Fu, Youming Yu, Binfu Bao. "Polyaniline Coated Boron Doped Biomass Derived Porous Carbon Composites for Supercapacitor Electrode Materials", Industrial & Engineering Chemistry Research, 2015<br>Publication | <1% |
| 23 | Submitted to Yonsei University | |

Student Paper <1%

24 Sook-Keng Chang, Zulkarnain Zainal. "Activated Carbon for Supercapacitors", Elsevier BV, 2019 <1%
Publication

25 Submitted to University College London <1%
Student Paper

26 Mylena Junqueira Pinto Brito, Mateus Pereira Flores Santos, Evaldo Cardozo de Souza, Leandro Soares Santos et al. "Development of activated carbon from pupunha palm heart sheaths: effect of synthesis conditions and its application in lipase immobilization", Journal of Environmental Chemical Engineering, 2020 <1%
Publication

27 Basri, N.H., M. Deraman, S. Kanwal, I.A. Talib, J.G. Manjunatha, A.A. Aziz, and R. Farma. "Supercapacitors using binderless composite monolith electrodes from carbon nanotubes and pre-carbonized biomass residues", Biomass and Bioenergy, 2013. <1%
Publication

28 Mujian Xia, Dongdong Gu, Chenglong Ma, Hongyu Chen, Hongmei Zhang. "Microstructure evolution, mechanical response and underlying thermodynamic mechanism of multi-phase strengthening WC/Inconel 718 composites using <1%

selective laser melting", Journal of Alloys and Compounds, 2018
Publication

| | | |
|---|---|---|
| 29 | Hualin Lin, Yeping Liu, Zhexin Chang, Song Yan, Shunchang Liu, Sheng Han. "A new method of synthesizing hemicellulose-derived porous activated carbon for high-performance supercapacitors", Microporous and Mesoporous Materials, 2019<br>Publication | <1% |
| 30 | www.ise-online.org<br>Internet Source | <1% |
| 31 | Submitted to King Fahd University for Petroleum and Minerals<br>Student Paper | <1% |
| 32 | Yulin Wang, Qingli Qu, Shuting Gao, Guosheng Tang, Kunming Liu, Shuijian He, Chaobo Huang. "Biomass derived carbon as binder-free electrode materials for supercapacitors", Carbon, 2019<br>Publication | <1% |
| 33 | Jarosław Serafin, Martyna Baca, Marcin Biegun, Ewa Mijowska et al. "Direct conversion of biomass to nanoporous activated biocarbons for high CO2 adsorption and supercapacitor applications", Applied Surface Science, 2019<br>Publication | <1% |

| | | |
|---|---|---|
| 34 | Peng Song, Xiaoping Shen, Wenfeng He, Lirong Kong, Xiaome He, Zhenyuan Ji, Aihua Yuan, Guoxing Zhu, Na Li. "Protein-derived nitrogen-doped hierarchically porous carbon as electrode material for supercapacitors", Journal of Materials Science: Materials in Electronics, 2018<br>Publication | <1% |
| 35 | Ali Ehsani, Hamidreza Parsimehr. "Electrochemical energy storage electrodes from fruit biochar", Advances in Colloid and Interface Science, 2020<br>Publication | <1% |
| 36 | Yazhi Liu, Gaoran Li, Yi Guo, Yulong Ying, Xinsheng Peng. "Flexible and Binder-Free Hierarchical Porous Carbon Film for Supercapacitor Electrodes Derived from MOFs/CNT", ACS Applied Materials & Interfaces, 2017<br>Publication | <1% |
| 37 | Joseph Osafo Eduah, Stephan Weck Henriksen, Eric Kwesi Nartey, Mark Kofi Abekoe, Mathias Neumann Andersen. "Nonlinear sorption of phosphorus onto plant biomass-derived biochars at different pyrolysis temperatures", Environmental Technology & Innovation, 2020<br>Publication | <1% |
| 38 | www.scientific.net<br>Internet Source | <1% |

| | | |
|---|---|---|
| 39 | Daniel I. Arango, Zulamita Zapata-Benabithe, Erika C. Arenas, Juan C. Perez-Osorno. "Influence of surface modification with nitric acid on electrochemical performance of agroindustrial waste-based activated carbon", Journal of Materials Science: Materials in Electronics, 2018<br>Publication | <1% |
| 40 | cdmf.org.br<br>Internet Source | <1% |
| 41 | Prabaharan, S.R.S.. "Nanostructured mesoporous carbon as electrodes for supercapacitors", Journal of Power Sources, 20061020<br>Publication | <1% |
| 42 | dspace.nm-aist.ac.tz<br>Internet Source | <1% |
| 43 | Peifeng Yu, Yeru Liang, Hanwu Dong, Hang Hu, Simin Liu, Lin Peng, Mingtao Zheng, Yong Xiao, Yingliang Liu. "Rational Synthesis of Highly Porous Carbon from Waste Bagasse for Advanced Supercapacitor Application", ACS Sustainable Chemistry & Engineering, 2018<br>Publication | <1% |
| 44 | Farma, R., M. Deraman, A. Awitdrus, I.A. Talib, E. Taer, N.H. Basri, J.G. Manjunatha, M.M. | <1% |

Ishak, B.N.M. Dollah, and S.A. Hashmi. "Preparation of highly porous binderless activated carbon electrodes from fibres of oil palm empty fruit bunches for application in supercapacitors", Bioresource Technology, 2013.
Publication

| | | |
|---|---|---|
| 45 | aip.scitation.org<br>Internet Source | <1% |
| 46 | jbcs.sbq.org.br<br>Internet Source | <1% |
| 47 | Paul Thomas, Chin Wei Lai, Mohd Rafie Bin Johan. "Recent developments in biomass-derived carbon as a potential sustainable material for super-capacitor-based energy storage and environmental applications", Journal of Analytical and Applied Pyrolysis, 2019<br>Publication | <1% |
| 48 | centaur.reading.ac.uk<br>Internet Source | <1% |
| 49 | Beatriz M Marim, Janaina Mantovan, Gina AG Giraldo, Suzana Mali. "Environmentally friendly process based on a combination of ultrasound and peracetic acid treatment to obtain cellulose from orange bagasse", Journal of Chemical Technology & Biotechnology, 2020 | <1% |

Publication

| | | |
|---|---|---|
| 50 | Oleg Yu. Posudievsky, Olga A. Kozarenko, Vyacheslav S. Dyadyun, Igor E. Kotenko, Vyacheslav G. Koshechko, Vitaly D. Pokhodenko. "Mechanochemically prepared polyaniline and graphene-based nanocomposites as electrodes of supercapacitors", Journal of Solid State Electrochemistry, 2018<br>Publication | <1% |
| 51 | Guangguang Dai, Lei Zhang, Yiliang Liao, Ying Shi, Jianjun Xie, Fang Lei, Lingcong Fan. "Multi-Scale Model for Describing the Effect of Pore Structure on Carbon-Based Electric Double Layer", The Journal of Physical Chemistry C, 2020<br>Publication | <1% |
| 52 | Nannan Guo, Min Li, Yong Wang, Xingkai Sun, Feng Wang, Ru Yang. "Soybean Root-Derived Hierarchical Porous Carbon as Electrode Material for High-Performance Supercapacitors in Ionic Liquids", ACS Applied Materials & Interfaces, 2016<br>Publication | <1% |
| 53 | Liu Wan, Ping Song, Jiaxing Liu, Dequan Chen, Rui Xiao, Yan Zhang, Jian Chen, Mingjiang Xie, Cheng Du. "Facile synthesis of nitrogen self- | <1% |

doped hierarchical porous carbon derived from pine pollen via MgCO3 activation for high-performance supercapacitors", Journal of Power Sources, 2019
Publication

54 "Trends in Manufacturing and Engineering Management", Springer Science and Business Media LLC, 2021 <1%
Publication

55 Cuhadaroglu, B.. "An experimental study on the effects of uniform injection through one perforated surface of a square cylinder on some aerodynamic parameters", Experimental Thermal and Fluid Science, 200708 <1%
Publication

56 Yahya, Mohd Adib, Z. Al-Qodah, and C.W. Zanariah Ngah. "Agricultural bio-waste materials as potential sustainable precursors used for activated carbon production: A review", Renewable and Sustainable Energy Reviews, 2015. <1%
Publication

57 Gaowa Liu, Lei Qiu, Hai Deng, Jubei Wang, Lei Yao, Libo Deng. "Ultrahigh surface area carbon nanosheets derived from lotus leaf with super capacities for capacitive deionization and dye adsorption", Applied Surface Science, 2020 <1%
Publication

| | | |
|---|---|---|
| 58 | Gaofeng Shi, Chao Liu, Guoying Wang, Xuefu Chen et al. "Preparation and electrochemical performance of electrospun biomass-based activated carbon nanofibers", Ionics, 2018<br>Publication | <1% |
| 59 | Gaur, V.. "Preparation and characterization of ACF for the adsorption of BTX and SO"2", Chemical Engineering & Processing, 200601<br>Publication | <1% |
| 60 | www.scribd.com<br>Internet Source | <1% |
| 61 | Xueyan Zhao, Olga Grätz, Jürgen Pionteck. "Effect of dopant and oxidant on the electrochemical properties of polyaniline/graphite nanoplate composites", Polymer International, 2018<br>Publication | <1% |
| 62 | akita-pu.repo.nii.ac.jp<br>Internet Source | <1% |
| 63 | "Handbook of Ecomaterials", Springer Nature, 2019<br>Publication | <1% |
| 64 | Xiao-Li Su, Ming-Yu Cheng, Lin Fu, Jing-He Yang, Xiu-Cheng Zheng, Xin-Xin Guan. "Superior supercapacitive performance of hollow activated carbon nanomesh with hierarchical | <1% |

structure derived from poplar catkins", Journal of Power Sources, 2017
Publication

---

65 Xiaoyan Zhao, Qian Wu, Chen Huang, Huidan Wei, Ruichen Wang, Chenyi Wang. "Highly efficient separation membrane based on cellulose acetate/chitosan fibrous composite substrate with activated carbon functional adsorption layer", Journal of Chemical Technology & Biotechnology, 2020 <1%
Publication

---

66 pubs.acs.org <1%
Internet Source

---

67 Erman Taer, Rika Taslim, Apriwandi, Agustino. "Carbon nanofiber electrode synthesis from biomass materials for supercapacitor applications", AIP Publishing, 2020 <1%
Publication

---

68 Hanwen Yang, Jie Zhou, Mengqi Wang, Shengji Wu, Wei Yang, Hui Wang. "From basil seed to flexible supercapacitors: Green synthesis of heteroatom-enriched porous carbon by self-gelation strategy", International Journal of Energy Research, 2020 <1%
Publication

---

69 Changde Ma, Jiakang Min, Jiang Gong, Xiaoguang Liu, Xueying Mu, Xuecheng Chen, <1%

Tao Tang. "Transforming polystyrene waste into 3D hierarchically porous carbon for high-performance supercapacitors", Chemosphere, 2020
Publication

---

70 Ming-En Liu, Chung-Hsi Chou, Lu Li, Yi-Hsieng Samuel Wu, Yi-Ling Lin, Dom-Gene Tu, Yi-Chen Chen. "Modulation effects of black-vinegar-based supplement against a high-fat dietary habit: antiobesity/hypolipidemic, antioxidative, and energy-metabolism effects", Journal of the Science of Food and Agriculture, 2020 <1%
Publication

---

71 Lin Qian, Feiqiang Guo, Xiaopeng Jia, Yinbo Zhan, Huiming Zhou, Xiaochen Jiang, Chao Tao. "Recent development in the synthesis of agricultural and forestry biomass-derived porous carbons for supercapacitor applications: a review", Ionics, 2020 <1%
Publication

---

72 "Supercapacitors Based on Carbon Nanomaterials", Carbon Nanomaterials for Advanced Energy Systems, 2015. <1%
Publication

---

73 Dong Xu, Ying Tong, Tingting Yan, Liyi Shi, Dengsong Zhang. "N,P-Codoped Meso-/Microporous Carbon Derived from Biomass <1%

Materials via a Dual-Activation Strategy as High-Performance Electrodes for Deionization Capacitors", ACS Sustainable Chemistry & Engineering, 2017

Publication

| | | | |
|---|---|---|---|
| Exclude quotes | On | Exclude matches | Off |
| Exclude bibliography | On | | |